Direct Generation of Polarization-Entangled Photon Pairs in a Poled Fiber

Eric Y. Zhu,* Zhiyuan Tang,† and Li Qian
Department of Electrical and Computer Engineering, University of Toronto, Toronto, Ontario, M5S 3G4, Canada

Lukas G. Helt, Marco Liscidini,‡ and J. E. Sipe
Department of Physics, University of Toronto, Toronto, Ontario, M5S 1A7, Canada

Costantino Corbari, Albert Canagasabey,§ Morten Ibsen, and Peter G. Kazansky
Optoelectronics Research Centre, University of Southampton, Southampton SO17 1BJ, United Kingdom
(Received 22 October 2011; published 21 May 2012)

We experimentally demonstrate the direct generation of polarization-entangled photon pairs in an optical fiber at room temperature by exploiting type-II phase-matched spontaneous parametric down-conversion. A second-order nonlinearity is artificially induced in the 17-cm-long weakly birefringent step-index fiber through the process of thermal poling, and quasi-phase-matching allows for the generation of entangled photons in the 1.5-micron telecom band when the fiber is pumped at 775 nm. A greater-than 80:1 coincidence-to-accidental ratio is achieved, limited mainly by multiphoton pair generation. Without the need to subtract accidentals or to compensate for walk-off, the raw two-photon interference visibility is found to be better than 95%, and violation of Bell's inequality is observed by more than 18 standard deviations. This makes for a truly alignment-free, plug-and-play source of polarization-entangled photon pairs.

DOI: 10.1103/PhysRevLett.108.213902 PACS numbers: 42.65.Lm, 03.67.Hk, 42.65.Wi, 42.81.Qb

Entanglement is the paradigmatic quantum-mechanical resource. Applications of bipartite photonic entanglement include quantum key distribution [1], state teleportation [2], and enhanced optical metrology [3]. Polarization entanglement is of particular interest, owing to the ease of control and detection of a photon's state of polarization in practical systems.

The first practical sources of polarization-entangled photon pairs were demonstrated in bulk nonlinear optical crystals [4] through the process of spontaneous parametric down-conversion (SPDC). However, such sources suffer from poor spatial mode definition and high coupling loss into single-mode fiber and other waveguide devices.

Waveguide-based sources [5–8] of correlated photon pairs allow for better transverse mode definition and offer better compatibility with integrated optics and modern fiber-based telecom infrastructures. In this respect, compact fiber-based sources of entangled photon pairs in the telecom band are highly desirable. Unfortunately, conventional fiber does not exhibit a second-order nonlinearity, and SPDC is forbidden. Thus, correlated photon pair generation in fiber is often realized through the third-order nonlinear process of spontaneous four-wave mixing (sFWM). However, photon pairs generated through sFWM are likely to overlap spectrally with Raman-scattered pump photons, which are a significant source of noise unless the waveguide is cryogenically cooled [9] or the fiber dispersion is drastically altered [10] so that there is a large spectral separation (> 40 THz) between signal and idler. Moreover, for both bulk crystal- and waveguide-based sources reported so far, additional steps to remove which-way information are required to *convert* the correlated photons into high-visibility polarization-entangled pairs [4,8,11,12], introducing greater complexity and higher loss.

By contrast, we demonstrate in this Letter the *direct* generation of polarization-entangled photon pairs in an optical fiber (at room temperature) with an artificially induced second-order nonlinearity. While previous reports of such poled fibers have demonstrated SPDC [13,14], they differ qualitatively from this Letter; in addition to a much-improved coincidence-to-accidental (CAR) ratio ($> 80{:}1$ vs $< 4{:}1$ previously), the key feature of our approach is to exploit type-II phase-matching [15] and a weak fiber birefringence [16] to generate polarization-entangled photon pairs. Furthermore, the small polarization mode dispersion (≈ 60 fs/m) of the fiber results in both spectral and temporal which-way information being negligible, even for a nondegenerate pair of down-converted photons. Without the need for further preparation steps, the biphoton states at the output of the poled fiber are already polarization-entangled.

A second-order nonlinearity is induced along the length of our twin-hole step-index fiber (cross section shown in the inset of Fig. 1) through the process of thermal poling [17–19]. This involves the creation of a frozen-in dc field $E^{(\mathrm{dc})}$ [18], oriented in the x (or H) direction, in the region surrounding the core. The presence of the dc field breaks the inversion symmetry of the fused silica, giving rise to an effective second-order nonlinearity [16,18]: $\chi^{(2)} = 3\chi^{(3)}E^{(\mathrm{dc})}$. Periodic UV erasure of the $\chi^{(2)}$ [20,21] along the longitudinal direction (z) of the fiber [$\chi^{(2)}(z + \Lambda) = \chi^{(2)}(z)$] allows for quasi-phase-matching (QPM). A QPM

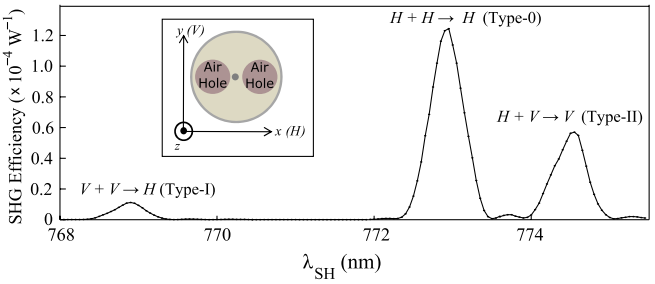

FIG. 1 (color online). Experimentally measured SHG spectrum of the PPSF. The fiber birefringence results in the spectral separation of three polarization-dependent phase-matchings. The type-II phase-matching (at ≈ 774.4 nm) is exploited for the generation of polarization-entangled photon pairs. The inset shows an illustrated cross section of the PPSF. The twin-hole step-index fiber has a core radius of 2.0 μm and a numerical aperture of 0.20. The principal axes x and y (or, equivalently, H and V) are labeled.

period $\Lambda = 52.8$ μm is chosen for our fiber to permit second-harmonic generation (SHG) at $\sim$775 nm in the LP_{01} transverse mode. The fiber birefringence and symmetry of the induced $\chi^{(2)}$ tensor [16] result in three spectrally separated SHG phase-matchings (Fig. 1). Pumping the now *periodically* poled silica fiber (PPSF) at 774.4 nm results in the production of type-II down-converted photon pairs centered at 1548.8 nm, also in the LP_{01} mode. Note that selecting other values for the poled fiber's QPM period will allow [22] for phase-matched down-conversion at other wavelengths.

The spectral brightness [23] for type-II SPDC in our PPSF is proportional to $\frac{(\chi^{(2)}_{yxy})^2 \mathcal{L}^2}{\mathcal{A}_{\text{eff}}}$. The tensor element $\chi^{(2)}_{yxy}[= \chi^{(2)}_{yxy}(-2\omega; \omega, \omega)]$ is responsible for the type-II phase-matched processes, and its magnitude has been found to be 0.022 pm/V from the SHG efficiency (Fig. 1). The length of the PPSF, $\mathcal{L}$, is 17 cm; $\mathcal{A}_{\text{eff}}$ (29 μm^2) is the modal overlap between the signal, idler, and pump photons. The total brightness of the source is obtained by integrating the expression (with appropriate prefactors) over the SPDC bandwidth; this bandwidth is computed from the modal dispersion of the fiber and shown in Fig. 2(a) as a function of the pump wavelength.

The inset of Fig. 2(a) redraws the tuning curve as a function of the signal and idler wavelengths, revealing that the generated biphotons are, in general, spectrally entangled. We must then write the biphoton state as $\int \phi(\omega_s, \omega_i)(|H, \omega_s\rangle|V, \omega_i\rangle + |V, \omega_s\rangle|H, \omega_i\rangle)d\omega_s d\omega_i$, where $\phi(\omega_s, \omega_i)$ is the joint spectral amplitude [15], ω_s (ω_i) is the signal (idler) frequency, and $H(V)$ is one of the PPSF's principal polarization axes. This spectral entanglement can be exploited [24] as a means of distributing polarization-entangled biphotons to multiple parties via narrowband wavelength-division multiplexing (WDM).

Tuning the pump wavelength to 774.6 nm [Fig. 2(a)], we can deterministically separate the two branches (signal and idler) of the down-converted photons into the C ("conventional," 1500–1565 nm) and L ("long," 1567–1610 nm)

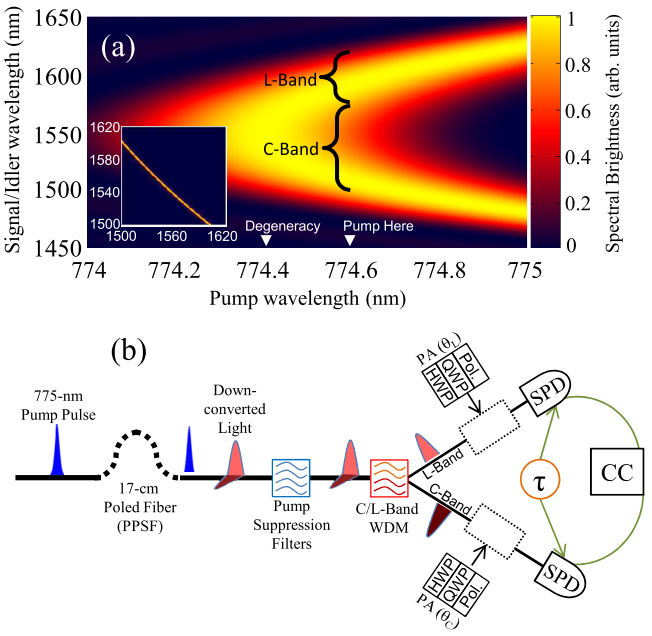

FIG. 2 (color online). (a) Theoretical tuning curve for type-II SPDC in our PPSF. Detuning the pump to longer wavelengths results in the production of nondegenerate photon pairs that can be spectrally separated into the C (1500–1565 nm) and L bands (1567–1610 nm). The inset shows the joint spectral intensity plotted as a function of the signal and idler wavelengths; note that the photons are highly anticorrelated in wavelength. (b) Experimental setup: The poled fiber is pumped by a mode-locked Ti:Sapph source (not shown). C and L band WDMs spectrally separate the down-converted photon pairs, which are then detected by a pair of single-photon detectors (SPDs). The coincidence counts (CCs) are recorded by a digital circuit. Polarization analyzers (PAs) are added to the setup to demonstrate polarization entanglement. Each PA consists of a free-space achromatic half- (HWP) and quarter-wave plate (QWP) and a polarizer (Pol).

spectral bands using coarse WDM filters. The spectral entanglement of the biphoton state can be ignored for the purposes of the measurements reported in this Letter, and we can denote the state with the shorthand

$$|\Psi^+\rangle = |H\rangle_C|V\rangle_L + |V\rangle_C|H\rangle_L, \quad (1)$$

where the subscript C (L) refers to the photon being in the C band (L band).

To generate the polarization-entangled photon pairs, a mode-locked (81.6 MHz, 10 ps pulsewidth) Ti:Sapph laser [not shown in Fig. 2(b)] is used as the pump, with its polarization adjusted to align to the slow axis (V) of the PPSF at the fiber input. Note that a Ti:Sapph is not required and can be replaced by a compact pulsed diode laser. At the output end of the PPSF, fiber-pigtailed pump suppression filters reduce the pump power by >110 dB, at an insertion loss of 4.3 dB for the down-converted light. This is then followed by a cascaded set of C/L band WDMs mentioned above, the insertion loss of which is 0.7 dB in the C band,

and 1.1 dB in the L band. All fiber pigtails used are Corning SMF28 single-mode fiber.

Two gated Geiger-mode InGaAs/InP single-photon avalanche photodiodes (SPDs) with measured quantum efficiencies of 10% (C band) and 6% (L band) are used for coincidence measurements. They are both triggered by the Ti-Sapph sync-out signal after it is frequency-divided to $f_{\text{trig}} = 5.1$ MHz. An adjustable relative delay τ between the two trigger signals can be introduced electronically. A digital logic circuit records the coincidence counts (CCs) of the two detectors.

The relative delay τ is varied over two periods (> 26 ns) of the pump pulse train to measure both CCs and accidental coincidence events [Fig. 3(a)]. Pump pulse energy is set at 210 pJ. Accidentals are averaged over the top three values in each accidental peak, and the CAR is found to be greater than 80:1.

Measurements similar to Fig. 3(a) are repeated at other pump energies. The CCs are found to scale linearly with pulse energy [Fig. 3(b)], and the slope of the linear fit yields a pair generation rate of 1.24×10^{-2} pairs/nJ per pulse, after correcting for insertion losses and quantum efficiencies of the SPDs. The average accidental counts (per second) are found to agree well with the formula $\frac{N_C \times N_L}{f_{\text{trig}}}$, where N_C (N_L) is the singles counts (per second) of the SPD in the C band (L band). Figure 3(c) shows the CAR plotted as a function of pump pulse energy, with the accidentals calculated using this formula to minimize the statistical uncertainties when the measured accidental rates are low. The results indicate that Raman noise and other noise contributions are negligible; the lower CAR at higher power is due mainly to multiphoton pair generation.

To demonstrate the polarization-entangled nature of the down-converted photon pairs, free-space polarization analyzers (PAs) are inserted as shown in Fig. 2(b). Each PA consists of achromatic wave plates [a quarter-wave plate (QWP) and a half-wave plate (HWP)] and a polarizer on rotatable mounts and has an insertion loss of 1.5 dB. The QWP and HWP act as polarization controllers and are configured so that, when the axis of the polarizer angle is set to 0°, the projected state is H-polarized.

Two-photon interference (TPI) measurements are performed [Fig. 3(d)], also at a pulse energy of 210 pJ. The C band polarizer is set to either $\theta_C = 0°$ (H) or $\theta_C = 45°$ (D), while the angle on the L band polarizer (θ_L) is swept over a range of more than 270°, in 22.5° increments.

Each set of TPI fringes is curve-fitted to a raised sinusoid, from which the visibility $\mathcal{V}$ is then calculated. Visibilities higher than 71% in both the H and D bases mean that the biphoton state is entangled. The visibilities $\mathcal{V}$ are found to be $97.4 \pm 2.1\%$ and $97.3 \pm 2.1\%$ in the H-V and D-A fringes, respectively. We emphasize that these are *raw* visibilities; accidental coincidences have not been subtracted. Calculating the S parameter [25] from the fringe visibilities [$S = \sqrt{2}(\mathcal{V}_H + \mathcal{V}_D)$], we obtain $S = 2.75 \pm 0.04$, which violates Bell's inequality by more than 18 standard deviations.

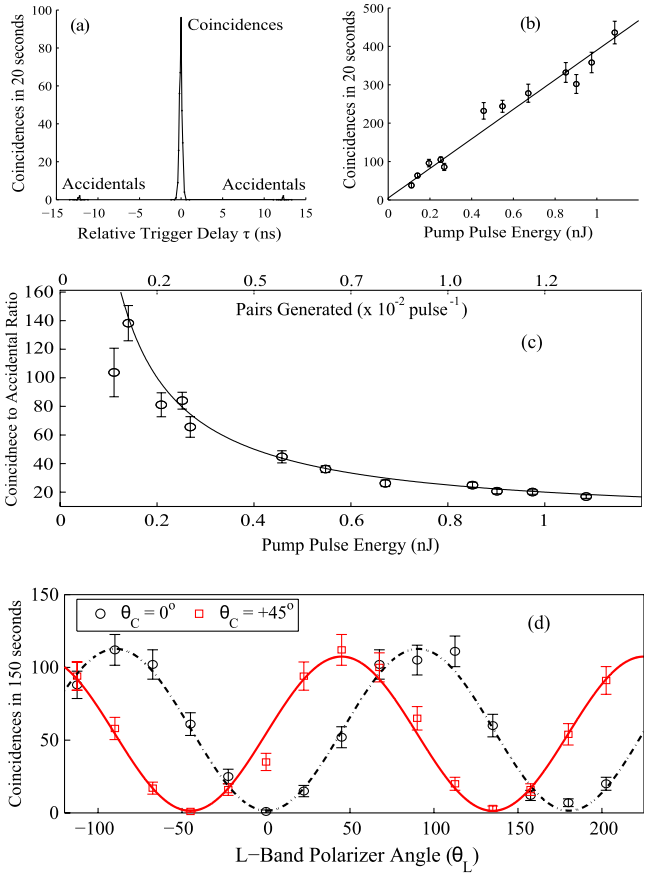

FIG. 3 (color online). (a) The relative delay τ between the two SPD trigger signals is varied to measure both accidentals and CCs. With a pump pulse energy of 210 pJ, the CAR is found to be in excess of 80:1. (b) CCs scale linearly with pump pulse energy, yielding a pair generation rate of 1.24×10^{-2} pairs/nJ per pulse. (c) The CAR is plotted for various pump pulse energies. (d) TPI results for the triplet state $|HV\rangle + |VH\rangle$. Visibilities of $97.4 \pm 2.1\%$ and $97.3 \pm 2.1\%$ are observed in the H-V (○) and D-A (□) bases (respectively), demonstrating polarization entanglement.

The SPDC brightness of our PPSF is lower than other sources due in part to its significantly lower $\chi^{(2)}$ (0.022 pm/V compared to 30 pm/V for periodically poled lithium niobate). A brighter PPSF source can be achieved by inducing a larger $\chi^{(2)}$ or increasing the length of the poled fiber. The poor detection efficiency of the SPDs and the large discrepancy between their trigger frequency (5.1 MHz) and the pump repetition rate (81.6 MHz) are also to blame; the two effects result in more than 99% of the generated photon pairs going undetected. Higher CAR and fringe visibilities may also be possible with better spectral filtering of the signal and idler photons; currently, the C and L band WDMs do not efficiently separate the signal or idler photons, with a significant number of pairs residing wholly in the C band [Fig. 2(a)]. The SPD dark

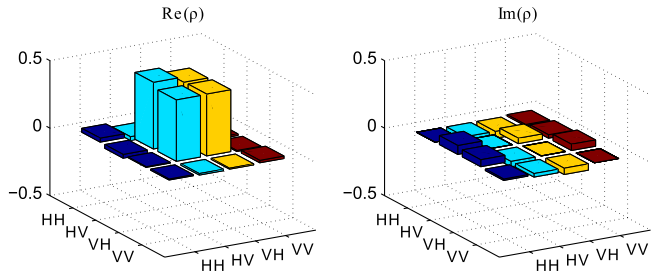

FIG. 4 (color online). The real and imaginary parts of the density matrix ρ for the triplet-state $|\Psi^+\rangle$ state, as reconstructed from quantum-state tomography. A fidelity $F = \langle\Psi^+|\rho|\Psi^+\rangle$ of 93.1% is obtained.

counts do not contribute significantly ($< 10\%$ of the singles counts) to the accidentals.

Transforming from one maximally entangled Bell state to another requires only a local Pauli operation (σ_x, σ_y, σ_z) on the polarization degree of freedom of one of the photons [4]. In our case, this can be done by adjusting the HWP and QWP in the L band PA. The triplet state $|HV\rangle + |VH\rangle$ is transformed to the other three Bell states, and visibilities exceeding 84% are observed in both the H-V and D-A bases.

Finally, quantum-state tomography [26,27] is performed on the triplet state $|\Psi^+\rangle$. Twenty-four coincidence measurements are made, for different combinations of the C band $\{H, V, D, R\}$ and L band polarizations $\{H, V, D, A, L, R\}$. The reconstructed density matrix ρ (Fig. 4) is found to have a concurrence [28] of 0.887 ± 0.052 and a fidelity ($F = \langle\Psi^+|\rho|\Psi^+\rangle$) of 93.1%, with the triplet state $|\Psi^+\rangle$.

In conclusion, we have demonstrated the *direct* generation of polarization-entangled photon pairs in a weakly birefringent periodically poled fiber by exploiting type-II SPDC, without the need for walk-off compensation or interferometric schemes to remove which-way information. The PPSF source exhibits high raw TPI visibilities ($> 95\%$) and high concurrence (0.887). This simple, rugged fiber-based, plug-and-play source of polarization-entangled photon pairs makes the implementation of quantum systems (e.g., quantum key distribution and quantum-enhanced sensing) possible at reduced complexity.

We thank Professor Hoi-Kwong Lo and Dr. Bing Qi for helpful discussions and acknowledge the Natural Sciences and Engineering Research Council of Canada (NSERC) for the funding of this project.

*eric.zhu@utoronto.ca
†Also at Department of Physics, University of Toronto, Toronto, Ontario, M5S 1A7, Canada.
‡Present address: Department of Physics, University of Pavia, Via Bassi 6, I-27100 Pavia, Italy.
§Present address: Optical Communications Group, University of New South Wales, Sydney, New South Wales 2053, Australia.

[1] T. Jennewein, C. Simon, G. Weihs, H. Weinfurter, and A. Zeilinger, Phys. Rev. Lett. **84**, 4729 (2000).
[2] D. Bouwmeester, J. Pan, K. Mattle, M. Eibl, H. Weinfurter, and A. Zeilinger, Nature (London) **390**, 575 (1997).
[3] A. F. Abouraddy, M. B. Nasr, B. E. A. Saleh, A. V. Sergienko, and M. C. Teich, Phys. Rev. A **65**, 053817 (2002).
[4] P. G. Kwiat, K. Mattle, H. Weinfurter, A. Zeilinger, A. V. Sergienko, and Y. Shih, Phys. Rev. Lett. **75**, 4337 (1995).
[5] Q. Zhang, X. Xie, H. Takesue, S. W. Nam, C. Langrock, M. M. Fejer, and Y. Yamamoto, Opt. Express **15**, 10 288 (2007).
[6] M. Fiorentino, S. M. Spillane, R. G. Beausoleil, T. D. Roberts, P. Battle, and M. W. Munro, Opt. Express **15**, 7479 (2007).
[7] H. Takesue, Y. Tokura, H. Fukuda, T. Tsuchizawa, T. Watanabe, K. Yamada, and S. Itabashi, Appl. Phys. Lett. **91**, 201108 (2007).
[8] T. Zhong, X. Hu, F. N. C. Wong, K. K. Berggren, T. D. Roberts, and P. Battle, Opt. Lett. **35**, 1392 (2010).
[9] H. Takesue and K. Inoue, Opt. Express **13**, 7832 (2005).
[10] J. Fan and A. Migdall, Opt. Express **15**, 2915 (2007).
[11] J. Chen, K. Fook Lee, X. Li, P. Voss, and P. Kumar, New J. Phys. **9**, 289 (2007).
[12] T. Kim, M. Fiorentino, and F. N. C. Wong, Phys. Rev. A **73**, 012316 (2006).
[13] G. Bonfrate, V. Pruneri, P. Kazansky, P. Tapster, and J. Rarity, Appl. Phys. Lett. **75**, 2356 (1999).
[14] K. Huy, A. Nguyen, E. Brainis, M. Haelterman, P. Emplit, C. Corbari, A. Canagasabey, P. Kazansky, O. Deparis, A. Fotiadi, P. Mégret, and S. Massar, Opt. Express **15**, 4419 (2007).
[15] L. G. Helt, E. Y. Zhu, M. Liscidini, L. Qian, and J. E. Sipe, Opt. Lett. **34**, 2138 (2009).
[16] E. Y. Zhu, L. Qian, L. G. Helt, M. Liscidini, J. E. Sipe, C. Corbari, A. Canagasabey, M. Ibsen, and P. G. Kazansky, Opt. Lett. **35**, 1530 (2010).
[17] R. Myers, N. Mukherjee, and S. Brueck, Opt. Lett. **16**, 1732 (1991).
[18] P. Kazansky and P. Russell, Opt. Commun. **110**, 611 (1994).
[19] A. Canagasabey, C. Corbari, A. V. Gladyshev, F. Liegeois, S. Guillemet, Y. Hernandez, M. V. Yashkov, A. Kosolapov, E. M. Dianov, M. Ibsen, and P. G. Kazansky, Opt. Lett. **34**, 2483 (2009).
[20] C. Corbari, A. Canagasabey, M. Ibsen, F. Mezzapesa, C. Codemard, J. Nilsson, and P. G. Kazansky, in *Optical Fiber Communication Conference and Exposition and The National Fiber Optic Engineers Conference* (IEEE, Piscataway, NJ, 2005), p. OFB3 [http://www.opticsinfobase.org/abstract.cfm?URI=OFC-2005-OFB3].
[21] H. An, S. Min, and S. Fleming, Proc. SPIE Int. Soc. Opt. Eng. **7846**, 784606 (2010).
[22] A. Strauss, U. Jauernig, V. Reichel, and H. Bartelt, Optik (Stuttgart) **121**, 490 (2010).

[23] Z. Yang, M. Liscidini, and J. E. Sipe, Phys. Rev. A **77**, 033808 (2008).

[24] W. Grice, R. S. Bennink, P. Evans, T. Humble, R. Pooser, J. Schaake, and B. Williams, in *Proceedings of the CLEO 2011 Conference on Laser and Electro-Optics, Baltimore, Maryland, 2011* (Optical Society of America, Washington, DC, 2011), p. JTuA5 [http://www.opticsinfobase.org/abstract.cfm?uri=CLEO:%20S%20and%20I-2011-JTuA5].

[25] J. F. Clauser, M. A. Horne, A. Shimony, and R. A. Holt, Phys. Rev. Lett. **23**, 880 (1969).

[26] D. F. V. James, P. G. Kwiat, W. J. Munro, and A. G. White, Phys. Rev. A **64**, 052312 (2001).

[27] J. Altepeter, E. Jeffrey, and P. Kwiat, Adv. At. Mol. Opt. Phys. **52**, 105 (2005).

[28] W. K. Wootters, Phys. Rev. Lett. **80**, 2245 (1998).